Applied Catalysis B: Environmental 147 (2014) 499–507

Contents lists available at ScienceDirect

Applied Catalysis B: Environmental

journal homepage: www.elsevier.com/locate/apcatb

Effects of size and shell thickness of TiO_2 hierarchical hollow spheres on photocatalytic behavior: An experimental and theoretical study

Min-Chiao Tsai[a], Jeng-Yi Lee[b], Po-Chin Chen[c], Yuan-Wei Chang[a], Ya-Chen Chang[a], Min-Han Yang[a], Hsin-Tien Chiu[c], I-Nan Lin[d], Ray-Kuang Lee[b], Chi-Young Lee[a,*]

[a] Department of Materials Science and Engineering, National Tsing Hua University, Hsinchu, Taiwan
[b] Institute of Photonics Technologies, National Tsing Hua University, Hsinchu, Taiwan
[c] Department of Applied Chemistry, National Chiao Tung University, Hsinchu, Taiwan
[d] Department of Physics, Tamkang University, New Taipei, Taiwan

ARTICLE INFO

Article history:
Received 9 June 2013
Received in revised form 3 September 2013
Accepted 22 September 2013
Available online 29 September 2013

Keywords:
Mie scattering
Hierarchical structure
Mie theory
Simulation
Ostwald ripening

ABSTRACT

Through a self-sacrificing template method, highly uniform hollow-spheres of TiO_2 anatase are synthesized with controllable diameter from 365 nm to 930 nm. Compared to large hollow spheres, a large enhancement in the photocatalytic activity is reported for the small hollow spheres (with a thickness of 50 nm). By extending Mie's scattering theory from solid- to hollow-spheres, for a spherical scatter with a diameter of 300–900 nm, theoretical calculation reveal that each singular hollow sphere has absorption power equivalent to a solid sphere as the shell thickness parameter reaches a critical value of 0.3–0.6. This critical thickness parameter is independent to the size of a single hollow sphere, demonstrating that hollow spheres have quantitative advantages over solid spheres of the same weight. Moreover, calculation supported that small hollow spheres have stronger absorption power than large hollow spheres due to higher thickness. This greatly enhance the performance of small hollow spheres under a photocatalytic test. Our theoretical results showed good agreement to the experimental measurements, and provided a framework for the design of hollow-sphere nano-particles for optimized absorption power.

1. Introduction

In the last few decades, nano-sized TiO_2 had attracted much interest due to its wide range of applications, which include lithium ion batteries [1,2], electrochromism [3,4], bio-technology [5,6] and photocatalysts [7–9]. Photocatalyst, which converts solar light into chemical energy, has attracted lots of attention, in particularly for its green energy applications. Instead of electrolyzing water, TiO_2 can be used as a major photocatalyst to decompose water into its constituents of hydrogen and oxygen, also functioning as a clean and recyclable energy access to hydrogen fuel [10,11]. To improve the photocatalytic activity, several methods are demonstrated, such as reducing the recombination of separated electron–hole pairs by blending various TiO_2 phases, or differing the size of TiO_2[12–14], depositing metal materials on a TiO_2 surface to form a heterojunction at the interface, introducing electron–hole scavengers or trapping sites to inhibit the recombination [15–19], and doping specific metal or non-metal elements to extend the absorption regime to visible wavelengths [20–23]. Additionally, enhancing light-harvest by utilizing hierarchical structured TiO_2 triggers great interests in recent years. As the size of the particle approaches the wavelength of incident light, resonance effect in light-scattering emerges, which is known as the Mie's scattering effect [24]. These special hierarchical structured materials keep both micron- and nano- scale inherent properties that could harvest more light by the scattering effect in micron structure whilst maintain high surface area as primary nano-sized particles. Inspired by materials in nature like seashells and plant seeds, the intricate structure and morphology have exhibited fascinating properties [25]. Instead of solid-spheres, hollow spheres have been widely used as adsorbents, delivery carriers, catalysts and biomedical detectors [26,27]. By considering hollow spheres, it is expected that synthesized material with a controlled structure should be better performing than that with an ordinary composition. It has been shown that hollow structures could enhance reaction efficiency remarkably for several applications such as in photocatalytic degradation of pollutants, dye-sensitized solar cells and H_2 generation, by increasing light utilization caused by resonance in the structure [28–34]. To meet the resonance condition, peaks in the scattering (extinction) spectrum only exist for some specific sizes. However, there remain a lack of published reports exploring the relationship between size effect and efficiency due to difficulty in synthesizing differently-sized uniform hollow spheres. In this study, highly uniform size-controllable TiO_2 hollow particles

* Corresponding author. Tel.: +886 3 5715131x42570.
E-mail address: cylee@mx.nthu.edu.tw (C.-Y. Lee).

0926-3373/$ – see front matter © 2013 Elsevier B.V. All rights reserved.
http://dx.doi.org/10.1016/j.apcatb.2013.09.033

are synthesized by using a self-sacrificing template method, in which amorphous TiO_2 spheres act as both the precursor and the template in *NaF* solution. The scattering properties and photocatalytic activity of these highly uniform size-controllable TiO_2 are reported for a range of different particle diameters from 365 nm to 930 nm. Compared to solid nano-particles (without a hollow -sphere structure), by crushing solid particle samples into powder form, a greatly enhanced photocatalytic activity is demonstrated for the hollow nano-particles, even though there is no large difference between the measured total surface areas in the crushed powders and hollow sphere nano-particles. By extending Mie's scattering theory, a quantitative analysis is developed for the extinction and absorption spectra of the hollow particles, in which reveal a crucial thickness for the hollow particles to enhance absorption. Our theoretical results not only give good agreement to experimental data, but also explain the mechanism for a counter-intuitive scattering property for these hollow-sphere nanoparticles. Based on the experimental and theoretical observations presented here, it provides a basis for the design of more complicated particle structures.

2. Experimental

2.1. Synthesis method

The method to prepare amorphous precursor spheres can be found in earlier work [5,35]. In brief, various sizes of nano-particles are synthesized using titanium isopropoxide (TTIP, 97%, Aldrich), valeric (99%), and butyric (99.5%) acids in anhydride alcohol (99.5%), which are all directly purchased from the Aldrich Company without pretreatment. First, valeric acid is injected into 20 mL ethanol. After that, 0.3 mL (1 mmol) TTIP is added. The solution is then heated to 85 °C for six hours under reflux in air. Solution with a variable amount of deionized water and 10 mL ethanol is added to induce hydrolysis and condensation, causing the particles to precipitate in a few minutes and making the solution turbid. The precipitate is recovered by centrifuging (1000 and 4000 rpm for micron- and submicron-sized spheres, respectively) and decanting the liquid. Through several washes in ethanol, with the centrifuging and decanting processes performed after each wash, the residual ethanol is pumped out by a vacuum oven at 50 °C for 30 min. Through a typical hydrothermal process, particles of a hollow shape are prepared as follows: 0.2 g of precursor sphere is dispersed in 25 mL *NaF* solution with different concentrations ranging from 0.00625 M to 0.2 M. The mixture is sealed in a 45 mL Teflon-lined stainless autoclave, followed by heat treatment at 190 °C for 18 h. The hydrothermal treatment transforms the amorphous precursor spheres into crystalline hierarchical hollow anatase spheres. The hollow-spheres are washed twice in ethanol and dried in a oven at 100 °C overnight.

2.2. Preparation for photocatalytic test

After mixing 0.01 g of the TiO_2 nano-particles with 50 mL of 25 ppm *Methylene Blue* solution, the solution is illuminated on top with a *Xe* bulb, from Osram Inc., operated at an output power of 180 W and maintained at a temperature of 20 °C. Samples of 0.5 mL are taken out every 5 min, filtered with a 0.2 mm filter, and diluted with 2 mL of deionized water. The filtrate is analyzed to determine the dye concentration, by a Hitachi UV-vis 3010 spectrophotometer.

3. Results and discussion

3.1. Hierarchical structured hollow spheres

Highly uniform TiO_2 anatase hollow-spheres are synthesized by using amorphous TiO_2 spheres as both the precursor and template. Fig. 1(a) shows the typical Scanning Electron Microscopy (SEM) image of our precursor spheres with a mean diameter of 514 nm.

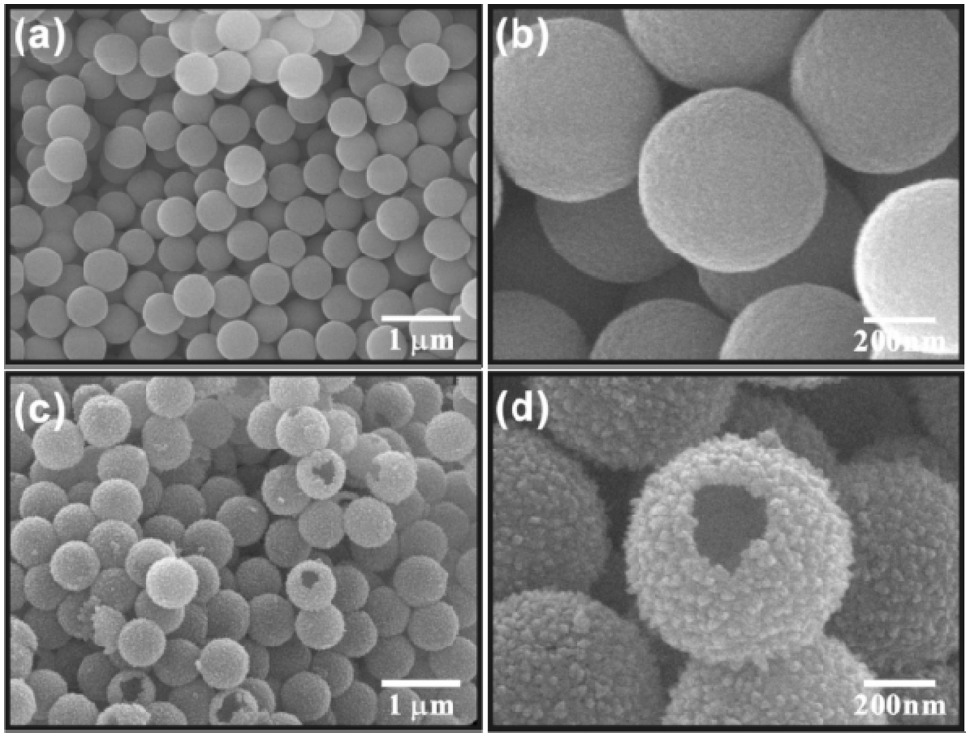

Fig. 1. SEM images at various magnifications of amorphous TiO_2 nano-particles in shape of (a and b) solid-spheres with an average diameter of 514 nm and (c and d) hollow spheres synthesized in 0.025 M NaF solution for 18 h with an average diameter of 590 nm.

The precursors are amorphous solid spheres with a smooth surface, which are clearly visible in high-magnification SEM image (Fig. 1(b)). After hydrothermal treatment using 0.025 M NaF solution, these nano-sized particles retained their spherical shape with a high level of uniformity. A slight increase in diameter of 590 nm, is also observed. Notably, the original smooth surface becomes a rough one and the solid spheres are transformed into hollow spheres, with clear evidence from the presence of broken spheres shown in Fig. 1(c) and (d).

To have a better knowledge on the formation process of the nano-sized hollow-spheres, Transmission Electron Microscope (TEM) is used to trace the formation of hollow-spheres at different reaction times, shown in Fig. 2. Initially, the solid spheres shrink rapidly and a thin shell with thickness of approximately 20 nm is formed on the surface of each sphere after 30 min, as observed in Fig. 2(a)–(c). A small increase in the particle size, from 520 nm to 570 nm, can be seen in Fig. 2(d). Thereafter, the precursor spheres completely disappear and hollow spheres form over 18 h, as displayed in Fig. 2(g), for which the diameter slowly increased to 590 nm approximately. From Fig. 2(b) and (c), unlike the starting amorphous solid-spheres with a smooth surface, the hollow spheres developed a very rough surface during the process. In contrast, as the nano-particles in the shell region grow, a smooth surface for hollow spheres is formed again (Fig. 2(h)). With High Resolution Transmission Electron Microscopy (HRTEM), the lattice fringe was measured to be 0.35 nm in the shell, which attributes to the anatase (1 0 1) plane, as shown in the inset of Fig. 2(i). The formed anatase nano-crystalline on the shell region is also confirmed by X-ray diffraction (XRD) pattern, see Fig. S1 in the supplementary information. The composed nano-crystalline anatase particles have a diameter around 7 nm, which is estimated using Scherrer's equation [36].

It is believed that the mechanism to form hollow-spheres involves a dissolution–reprecipitation process, *i.e.*, Ostwald ripening [37–39]. From the corresponding TEM images in Fig. 2 for different reaction times, our synthesis process can be viewed as a two-stage transformation. In the first stage, the amorphous TiO_2 reacts with F^- ions in the NaF solution to form H_2TiF_6 [40]. During this process, some of the TiO_2 spheres dissolve, resulting in the shrinking of particle diameter. Subsequently, H_2TiF_6 reacts with H_2O to generate titanium hydroxyl species. This hydrolysis reaction is then followed by the condensation reaction of titanium hydroxyl species, yielding anatase nano-particles to deposit on the surface of partially dissolved precursor spheres and form a shell around the hollow sphere. Overall, the amorphous precursor spheres change into hollow spheres composed of irregularly shaped nano-particles

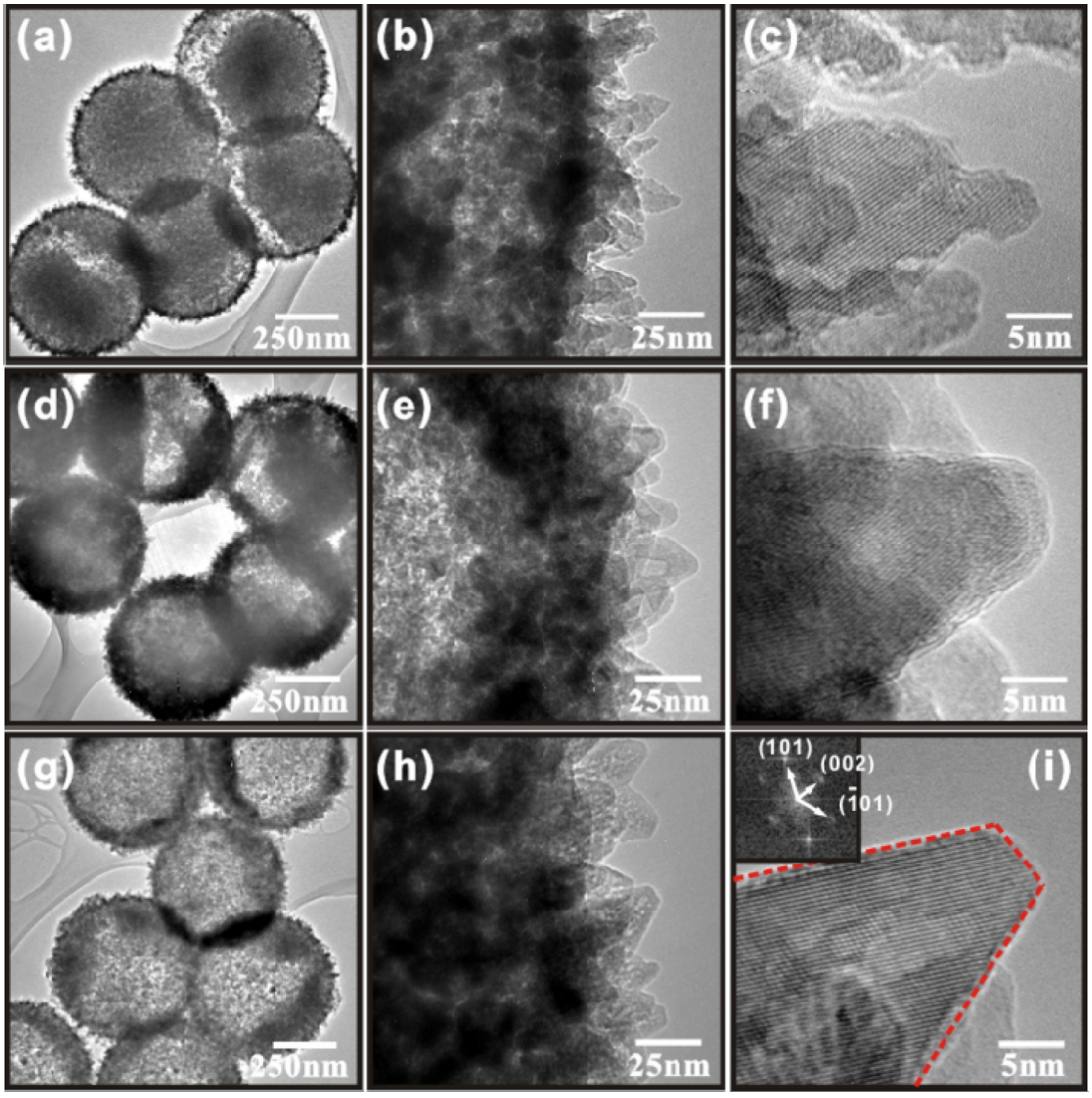

Fig. 2. TEM images of hollow anatase spheres taken during the synthesis process at different reaction times in *NaF* solution: (a–c) 0.5 h; (d–f) 6 h; and (g–i) 18 h.

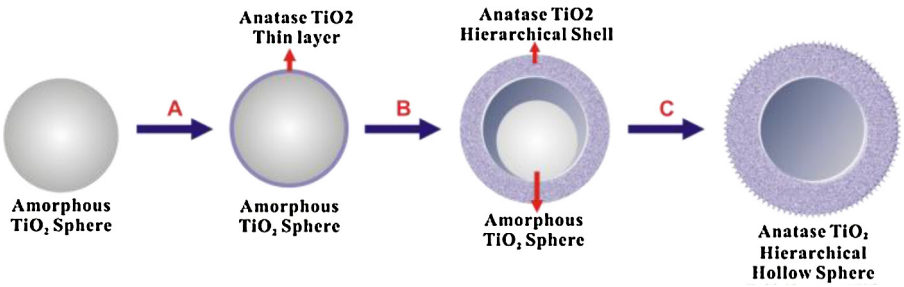

Scheme 1. Illustration of the two-stage transformation from amorphous TiO_2 spheres into anatase TiO_2 hierarchical hollow spheres, where step A indicates a thin layer consisted of anatase nano-particles forming on the surface of amorphous TiO_2 sphere, step B indicates the core of TiO_2 spheres shrinking and dissolving as nutrients for shell thickening, and step C indicates the shell continuously growing until the core TiO_2 spheres is exhausted.

on the surface through a typical Ostwald ripening process, in which small particles dissolve as nutrient for the growth of the larger particles to reduce total surface energy [41,42].

In the second stage, the irregularly shaped nano-crystalline particles grow slowly. From the ripening, only facet (1 0 1) sustains for a lower surface energy. In the final phase, the anatase nano-particles grow into the shape of hollow spheres, composed of rhomboid anatase, see Fig. 2(g). Notably, these two stages can happen simultaneously, despite the separation of entire process into different stages herein for a clearly descriptive purpose. When the facets of nano-crystalline particles are mostly recovered, some of the precursor spheres may remain intact inside the newly formed hollow-spheres, as a sphere-in-sphere structure shown in Fig. 2(d).

To elucidate the details in the shell region, we perform Barrett–Joyner–Halenda (BJH) pore size and volume analysis on the hollow spheres, see Fig. S2(a) in the supplementary information. Two peaks at 8 nmand 35 nm indicate that the hollow-spheres contain two kinds of pores of different sizes. The measurement suggests that each shell comprise of two groups of nano-particles, a large and a small pore coming from the fine-growth nano-particles at the interfaces of shells. The hollow spheres with a shell mixed with two kinds of pores can have a unique hierarchical structure, which gives a high surface area of 83 m^2/g by Brunauer–Emmett–Teller (BET) surface area analysis, see Fig. S2(b). Compared to the hollow spheres, crushed nano-particles have a similar BET surface of 74 m^2/g, but with different pore sizes of mainly 50 nm. The significant drop of peak intensity at 8 nm shows that the shells of the hollow-spheres are completely crushed. Based on experimental data above, Scheme 1 illustrate the two-stage transformation for synthesizing hollow-spheres as described. Worthy to note here that, compared to other known synthesis processes, the TiO_2 amorphous spheres here are treated not only as precursors but also as templates.

The effect of F^- ion concentration on the formation of hollow-spheres is also studied. As shown in Fig. 3, mesoporous spheres rather than hollow-spheres are obtained when the concentration of F^- ions is less than 0.0125 M. This observation is consistent with the findings of other investigations in which mesoporous spheres are synthesized under hydrothermal conditions without any additive [43,44]. With a higher F^- ion concentration, rod-like nano-crystalline particles grow on the surface of spheres, along the [0 0 1] direction anisotropically. In this scenario, (1 0 1)-truncated

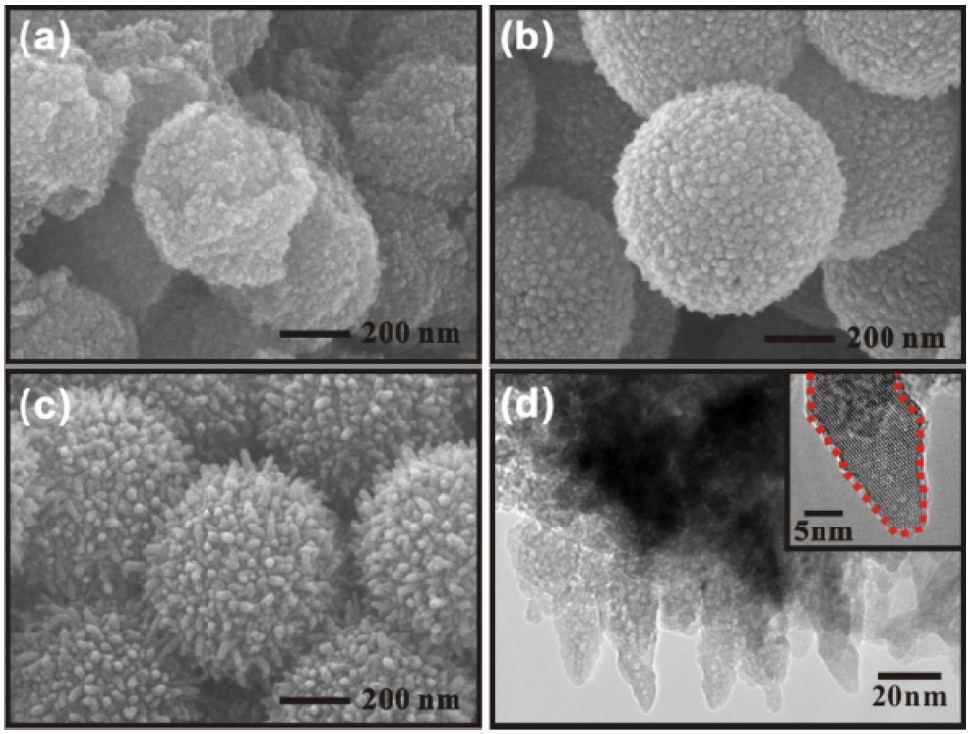

Fig. 3. SEM images of raw titania spheres hydrothermally treated with various concentrations of NaF solution: (a) 0.00625 M, (b) 0.0125 M and (c) 0.2 M, respectively. TEM image of spheres in 0.2 M NaF solution is shown in (d), with a HRTEM image in the inset.

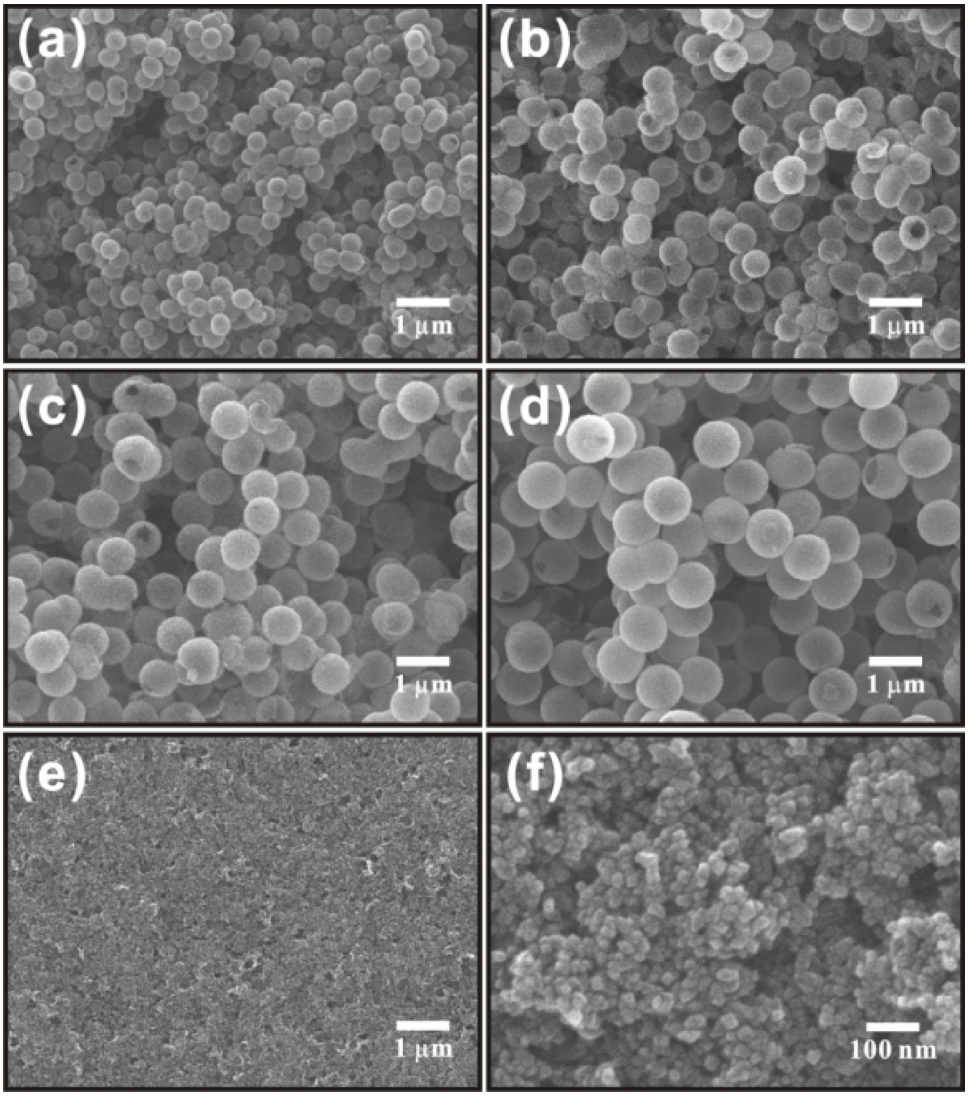

Fig. 4. SEM images of different sized hollow spheres used for photocatalytic test: (a) 365 nm, (b) 580 nm, (c) 780 nm and (d) 900 nm, respectively. The hollow spheres were crushed into nano-particles for comparison, as shown in (e) and (f).

hollow-spheres are produced, as shown in Fig. 3(c) and (d). Generally, the growth along a high index direction reduces the surface energy, resulting in the (1 0 1)-truncated particles such as bipyramids, diamonds, and bullets in the absence of surfactants [45]. However, F^- ions in the solution selectively and strongly bind on (0 0 1) facet as a surfactant, then substantially retard and stabilize the growth of (0 0 1) plane, resulting in the formation of (0 0 1)-truncated decahedral nano-particles [46,47]. In this work, (1 0 1)-truncated particles are obtained even when the F^- ion concentration is as high as 0.2 M. In this case, F^- ions did not bind to (0 0 1) plane due to the coexistence of Na^+ ions in the solution, and the growth of (0 0 1) plane was not largely retarded. Simulations of the absorption of Na^+ and F^- ions on the (0 0 1) plane support experimental results herein [48]. When the ratio of growth rate between (0 0 1) and (1 0 1) planes is slightly less than 2.7, rod-shaped particles with an almost fixed area in the exposed (0 0 1) and (1 0 1) surfaces can be obtained. Additionally, the expansion of (1 0 1) plane is not homogeneous when the total area of (1 0 1) plane reaches a critical value. After which, on the top of the growth front, it can produce a zigzag shape [45]. Thus, the nano-particles are elongated in the [0 0 1] direction, and extending the (1 0 1) plane, resulting in the zigzag shape as shown in the inset of Fig. 3(d).

3.2. Photocatalytic test

The photocatalytic activity of our TiO_2 hollow-spheres is performed through the photo-degradation of *Methylene Blue* (MB), with the synthesized hollow sphere nano-particles of different diameters, *i.e.*, from 365 nm to 930 nm, but with the same thickness of shell around 50 nm, which are shown in Fig. 4(a)–(d). Fig. 5 shows a plot of C/C_0 (where C is the final concentration and C_0 is the initial concentration) as a function of irradiation time of various sized hollow spheres. It reveals that the residual MB concentration after 30 min of irradiation decreases with decreasing particle size. In order to quantify the results, degradation rate constant was used for evaluating the effect of size on photocatalytic ability. Since the solution is dilute, we can assume that the photocatalytic behavior has a pseudo-first-order degradation rate constant, κ-value, which can be calculated by

$$\kappa = -\frac{\ln(C/C_0)}{\Delta t} \quad (1)$$

where C and C_0 are the corresponding final and initial concentrations of *Methylene Blue*, and Δt is the interacting time period. As a comparison, crushed hollow sphere nano-particles with the

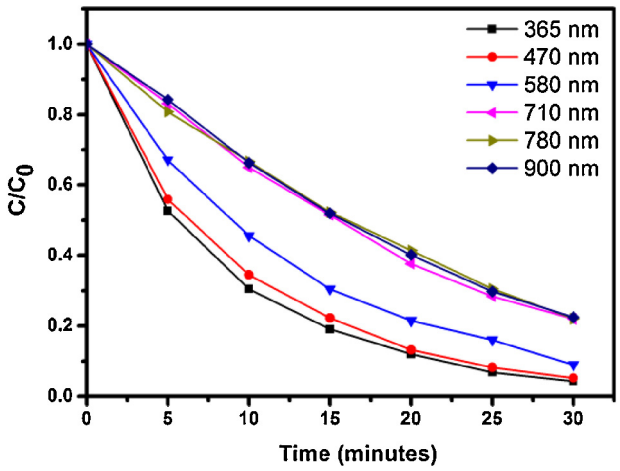

Fig. 5. Photocatalytic degradation test (C/C_0 *versus* irradiation time) of Methylene Blue for differently sized TiO_2 hollow spheres.

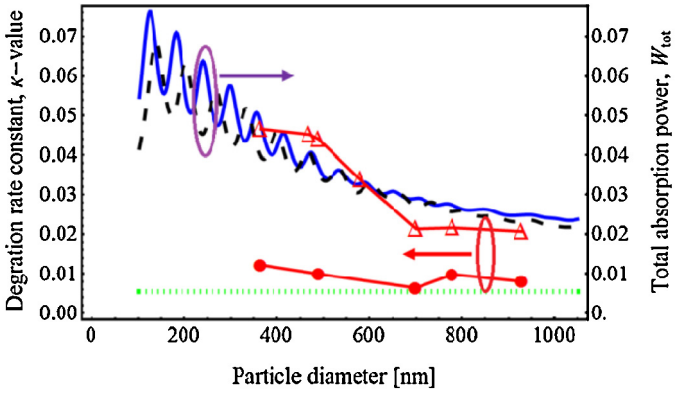

Fig. 6. Performance of photocatalytic activities, in terms of the experimental measurement of degradation rate constant, κ-value, for hollow sphere nano-particles of different diameters (marked by △). Numerical simulations of the total absorption power, W_{tot}, are shown for different incident wavelengths: $\lambda_0 = 350$ nm (solid-line) and 388 nm (dashed-line), with the thickness of shell in 50 nm. A reference sample, made by crushing the original hollow sphere particles into a powder with the same weight, is shown for the comparison with the experimental data marked by ● and its numerical simulations as a dotted-line.

same weight (powders) were tested for its photocatalytic activity under the same above conditions. It is clearly observed that no hollow spheres were present after crushing, as shown in Fig. 4(e) and (f). A comparison between hollow spheres and crushed samples is shown in Fig. 6, marked by △ and ●, respectively. This clearly demonstrates a significant difference between the two groups. In Fig. 6, one can see that the κ-value to measure photocatalytic activity which is enhanced for hollow spheres, when the particle diameter is less than 500 nm. Then this value drops gradually from 0.045 to 0.0225 as the diameter increases to 700 nm. However, the κ-value obtained by the crushed samples remains almost around 0.01 for all the cases, no matter what kind of the original hollow-spheres is smashed from. From our BET measurements shown in Fig. S2(b), our synthesized hollow-sphere nano-particles have almost the same total surface area (83 m^2/g) as that of crushed samples (74 m^2/g). Moreover, UV–vis diffuse reflectance spectra which is also included in the manuscript for evaluating photo-absorption of hollow spheres with different sizes from 360 nm to 800 nm (Fig. S3). The red shift of absorption edges of large hollow spheres were clearly observed, showing band gap of larger hollow spheres having slightly diminished, which indicates the larger hollow spheres possess wider photo-absorption range than smaller one and consequently, better photocatalytic performance

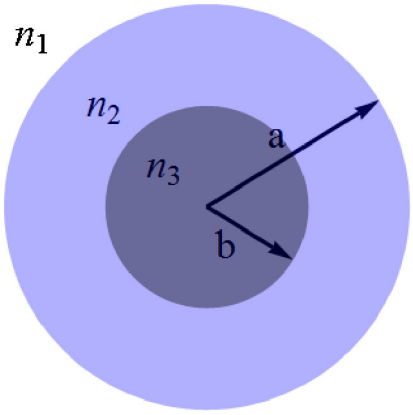

Scheme 2. Illustration of a hollow-sphere particle used in our theoretical model, with the refractive indexes in three different regions denoted by n_1, n_2, and n_3. The outer and inner radii are labeled by a and b, respectively.

might be expected. However, the anticipations of UV–vis spectra conflict against the photocatalytic performance results in Fig. 6, that the smaller hollow spheres have better photocatalytic performance. As a result of the above observation and discussion, we found that geometric parameters such as particle size and thickness of TiO_2 hollow spheres influence photocatalytic performance much more seriously. It would be demonstrated theoretically later, that hollow-spheres with an enough thickness and size effect can significantly enhance the photocatalytic behavior.

3.3. Theoretical model

To achieve a deeper understanding on the scattering properties and related thickness effect of hollow-spheres, we developed a theoretical model to quantitatively consider the scattering properties of hollow sphere nano-particles by extending Mie's scattering theory [49]. Based on Mie's scattering theory for a single solid sphere, we consider a single particle in the shape of a hollow sphere, as illustrated in Scheme 2. In this geometry, the refractive index of surrounding media is considered as real, n_1, and within the interior region of two different complex refractive indices (to include possible absorption effects) are denoted as n_2 and n_3. The outer and inner radii are labeled by 'a' and 'b', respectively. We also assumed that multiple scattering effects from other particles are negligible due to the dilute solution that we used in the photocatalytic performance here. Considering a monochromatic electromagnetic plane wave illuminating on such a hollow sphere, we can solve the scattering in the spherical coordinate.

For the surrounding media, there exist incident plane wave and scattering wave, whilst in the interior region, there are transmitted and internal refracted waves. By matching the boundary conditions, we found the corresponding coefficients for scattering, transmitted and internal refracted waves. To simplify our calculations, we only focused on the scattering wave in the far-field region. Subsequently, the rate of energy transported by the field per unit area, the Poynting vector, is used to calculate the absorption power of hollow-sphere particles through a volume integral, *i.e.*,

$$\frac{W_{abs}}{I_{in}} = \pi a^2 Q_{abs}(x, y) \tag{2}$$

where W_{abs} and Q_{abs} show the absorption power and related efficiency factor for absorption for a single hollow-sphere. Here, we introduced two size parameters for the outer and inner radii, *i.e.*, $x = 2\pi a/\lambda_0$ and $y = 2\pi b/\lambda_0$, respectively. The illuminated light in vacuum has the wavelength λ_0, and I_{in} is the incident intensity. The efficiency factor for absorption, $Q_{abs}(x,y)$, is related to the efficiency

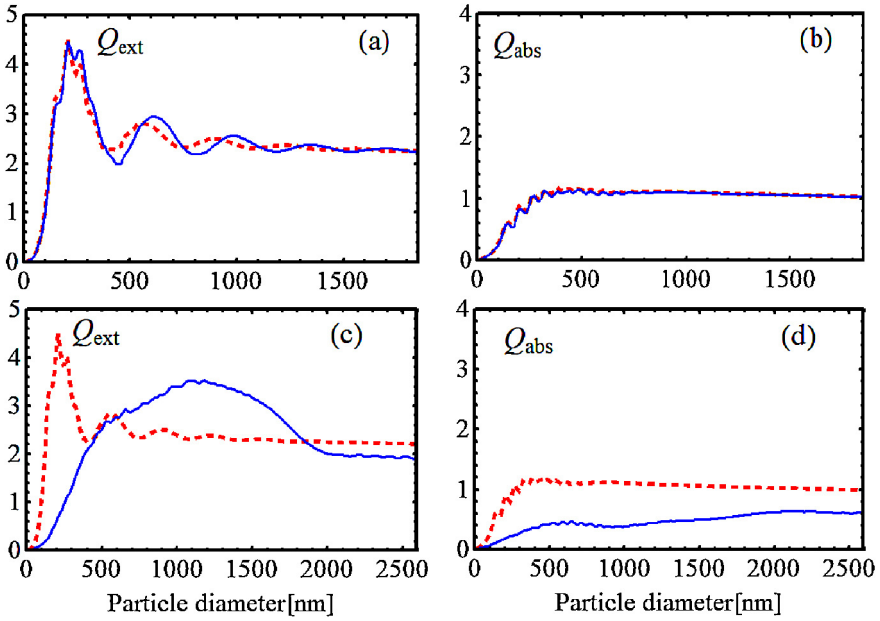

Fig. 7. Calculated efficiency factors for extinction and absorption, Q_{ext} and Q_{abs} for (a and b) thick ($\xi = 0.7$), and (c and d) thin ($\xi = 0.1$) hollow particles. Here, other parameters used are the incident light wavelength $\lambda_0 = 388$ nm, the refractive indexes $n_1 = 1.33$, $n_2 = 2.5 + 0.1i$ and $n_3 = 1.33$, respectively. The dashed-lines show the curve for a fully-filled solid-sphere as a reference.

factors for extinction and scattering, Q_{ext} and Q_{scat}, through the definition,

$$Q_{abs}(x, y) = Q_{ext}(x, y) - Q_{scat}(x, y) \tag{3}$$

where

$$Q_{ext} = \frac{2}{n_1^2 x^2} \sum_{l=1}^{\infty} (2l+1) \mathrm{Re}\{a_l^{E,s} - a_l^{H,s}\} \tag{4}$$

$$Q_{scat} = \frac{2}{n_1^2 x^2} \sum_{l=1}^{\infty} (2l+1) \{|a_l^{E,s}|^2 + |a_l^{H,s}|^2\} \tag{5}$$

with the corresponding scattering coefficients $a_l^{E,s}$ and $a_l^{H,s}$ to characterize the scattering waves related to the *E*- and *H*- fields, which have the explicit formulas given in the following

$$a_l^{E,s} = \frac{n_2 f_l^{111}(n_2 f_l^{132} V_l^2 + n_3 f_l^{032} V_l^3) + n_1 f_l^{011}(n_3 f_l^{032} V_l^1 + n_2 f_l^{132} V_l^4)}{n_3 f_l^{032}(n_1 g_l^{011} V_l^1 + n_2 g_l^{111} V_l^3) + n_2 f_l^{132}(n_2 g_l^{111} V_l^2 + n_1 g_l^{011} V_l^4)} \tag{6}$$

$$a_l^{H,s} = \frac{n_2 f_l^{032}(n_2 f_l^{011} V_l^1 + n_1 f_l^{111} V_l^3) + n_3 f_l^{132}(n_1 f_l^{111} V_l^2 + n_2 f_l^{011} V_l^4)}{n_3 f_l^{032}(-n_1 g_l^{011} V_l^1 - n_2 g_l^{111} V_l^3) + n_2 f_l^{132}(-n_2 g_l^{111} V_l^2 - n_1 g_l^{011} V_l^4)} \tag{7}$$

where

$$V_l^1 = -f_l^{122} g_l^{121} + f_l^{121} g_l^{122} \tag{8}$$

$$V_l^2 = -f_l^{022} g_l^{021} + f_l^{021} g_l^{022} \tag{9}$$

$$V_l^3 = f_l^{122} g_l^{021} - f_l^{021} g_l^{122} \tag{10}$$

$$V_l^4 = -f_l^{121} g_l^{022} + f_l^{022} g_l^{121} \tag{11}$$

Here, n_i, for $i = 1, 2, 3$, denotes the refractive indexes in three different regions. The corresponding spherical Bessel and spherical Hankel functions are presented by $j_l(z)$ and $h_l(z)$, respectively. To simplify the formulas, some shorthand notations are introduced in the following,

$$f_l^{ijk} \equiv \left(\frac{d}{dz}\right)^i [z j_l(z)]|_{z=n_j \alpha_k}$$

$$g_l^{ijk} \equiv \left(\frac{d}{dz}\right)^i [z h_l(z)]|_{z=n_j \alpha_k}$$

with $(d/dz)^0 = 1$, $(d/dz)^1 = d/dz$, $\alpha_1 = x$, and $\alpha_2 = y$, respectively. Based on the formulas from the extended Mie's scattering theory, given in Eqs. (4) and (5), we have shown the calculated efficiency factors for extinction and absorption, Q_{ext} and Q_{abs} for hollow-spheres in Fig. 7. To have a clear comparison with our synthesized hollow sphere nano-particles, instead of the normalized size parameters commonly adopted in the literature, we fixed the incident light wavelength at l0 = 388 nm, corresponding to the energy gap 3.2 eV for TiO_2 materials, and vary the particle diameters. By considering the photocatalytic activity performed in the water, we took $n_1 = 1.33$, $n_2 = 2.5 + 0.1i$, and $n_3 = 1.33$ in our simulations. As an extreme case by setting the inner radius $b = 0$, the calculated efficiency factors for extinction and absorption shown in the dashed-lines in Fig. 7, can be reduced to the accepted results for a fully-filled solid-sphere. With these dashed-lines, it not only justifies our extended Mie's theory, but also used as a reference in the comparison.

To identify the thickness effect, we also introduced a normalized thickness parameter defined as

$$\xi \equiv \frac{a - b}{a} \tag{12}$$

which varies from 0 to 1. In this case, for a complete empty sphere ($b = a$), we have $\xi = 0$; while for a fully-filled solid sphere ($b = 0$), we have $\xi = 1$. For example, one can fix the thickness parameter at $\xi = 0.7$ for the consideration of a *thick* hollow-sphere. As shown in Fig. 7(a) and (b), even though there exists a shift in the resonance peaks for the Mie's scattering, the corresponding efficiency factors for extinction and absorption for a hollow-sphere are almost

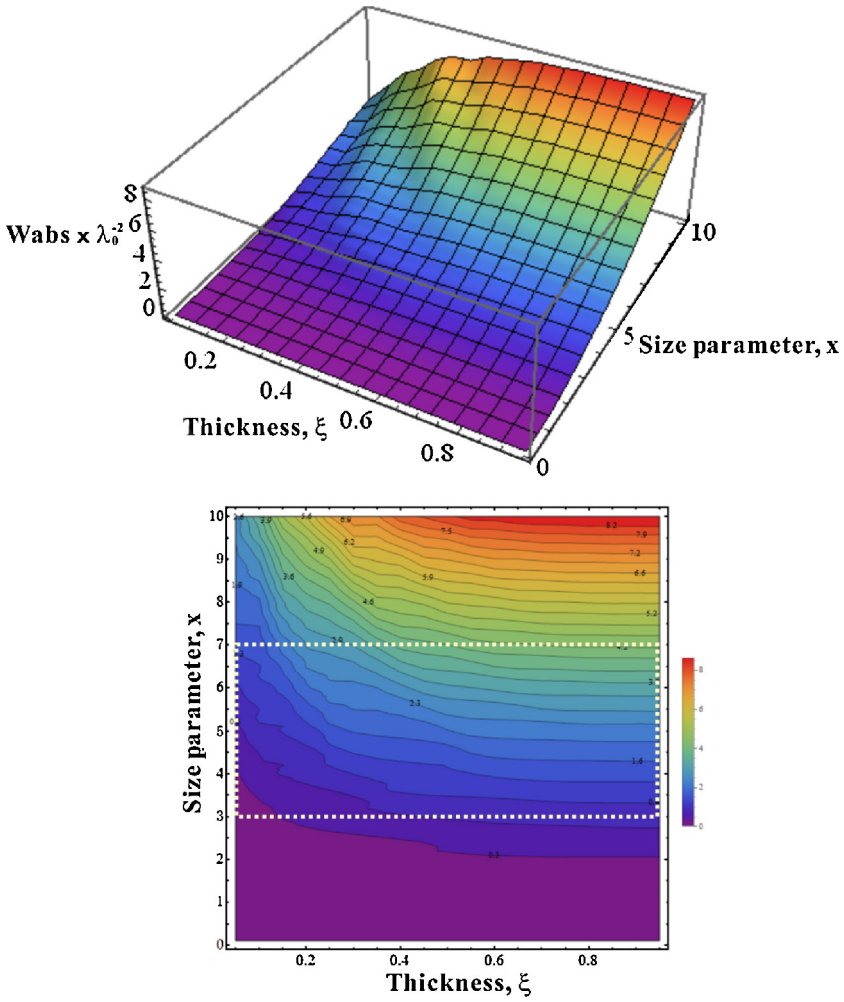

Fig. 8. Absorption power for a single hollow sphere, W_{abs}, is shown for different thickness parameter, ξ, and different size parameter, x in (a) 3D and (b) contour plots respectively. A clear transition from high absorption to low absorption is demonstrated between the colored and uncolored regions in the contour plot (b), where the number shown in the contour line is the value of scaled absorption power, W_{abs}/I_2^0.

the same as those of a fully-filled solid-sphere, *i.e.*, the dashed-lines in Fig. 7. In this case, we can say that the hollow-sphere is thick enough. In contrast, for a *thin* hollow sphere, such as the thickness parameter taken as $\xi = 0.1$ in Fig. 7(c) and (d), the extinction and absorption curves are significantly modified. Now, the first resonance peak in the efficiency factor for extinction is not only shifted notably but also broadened significantly, as shown in Fig. 7(c). Moreover, from Fig. 7(d), the corresponding efficiency for absorption also decreases dramatically. In this case, the scattering property of a hollow-sphere is totally different from those of a solid-sphere.

To have a further link with our experiments on photocatalytic performance of hollow spheres, we take the weight of photocatalyst into consideration. Applying the condition of same weight, the total absorption power for nano-particles, W_{tot}, can be calculated by including the total number of particles $N_{particle}$, *i.e.*,

$$W_{tot} \equiv N_{particle} \times \frac{W_{abs}}{I_{in}} \tag{13}$$

For particles in shape of a fully-filled solid-sphere, the total number of particles is $N_{solid\ particle} = 3M/4\pi\rho a^3$, for a given mass M, the known material density ρ, and the particle radius a. But for particles in shape of a hollow-sphere, with the outer and inner radii defined as a and b, the corresponding total number of particles becomes $N_{hollow\ particle} = 3M/4\pi\rho(a^3 - b^3)$. It can be understood that for the same weight, we have more particle numbers in shape of hollow spheres.

Numerical simulation of the absorption power for a single hollow sphere, W_{abs}, is shown in Fig. 8 for different thickness parameter, ξ, and different size parameter, x. From the contour plot in Fig. 8(b), a clear transition from high-absorption to low-absorption region can be seen. For a given hollow-sphere, when the shell of enough thickness, one has almost the same scattering properties as a single solid-sphere. By considering a spherical scatter with a diameter of 300–900 nm mostly observed in the reports (size parameter, $x = 3$–7 at wavelength of 350 nm of incident light as marked by a white dashed rectangle in Fig. 8(b)), our calculation shows that a hollow sphere has absorption power equivalent to a solid sphere when the shell thickness parameter reaches a critical value, 0.3–0.6. However, with a hollow structure, the total number of particles for hollow-spheres is larger than that of solid-spheres resulting in the enhancement of total absorption power. Instead, when the shell of a hollow sphere is too thin, the overall absorption power approaches to the value of crushed powders without any nano-structures even though the total number of particles increases.

Considering now the above theoretical results with the experimental measurement of photocatalytic activity in Fig. 6, the effect of the hollow structure of the particle on photocatalytic activity is demostrated. We assume that the measured photocatalytic

performance is dominated by the total absorption power through a linear relationship between the electron–hole recombination and total absorption power of TiO_2 nanoparticles. Other mechanisms, such as electron–hole migration or trapping process, are neglected at this stage. Our numerical results for the total absorption power are demonstrated for hollow spheres with shell size of 50 nm, but with different particle diameters. For wavelength around TiO_2 energy gap, such as the solid- and dashed-lines for the incident light wavelengths at λ_0 = 350 nm and 388 nm shown in Fig. 6, the calculated curves of total absorption power, W_{tot}, have a very similar tendency. That is, we have a very large value of absorption power when the diameter of hollow spheres is smaller than 500 nm. On the other hand, when the particle diameter is larger than 500 nm (*i.e.* when the hollow sphere is *thin*), the absorption power decreases. Furthermore, the absorption power for the case of crushed samples, by taking the particle diameter to 25 nm in simulations, can be viewed as a reference line (dotted-line in Fig. 6). In this way, our simulation curve depicts the low photocatalytic behavior of crushed TiO_2 samples. The comparison between our theoretical results and experimental data, the markers in Fig. 6, is in good agreement and confirms the enhancement of photocatalytic activity by using TiO_2 nano-particles in shape of hollow-spheres.

4. Conclusion

We reported experimental and theoretical scattering properties of highly uniform TiO_2 nano-particles in the shape of hollow spheres as photocatalyst. Our hollow sphere nano-particles are synthesized by a self-sacrificing template method in which the TiO_2 spheres act not only as a precursor but also as a template in NaF solution. With a controllable diameter in the hollow sphere, a size-dependent enhancement of photocatalytic activity is demonstrated and compared quantitatively with an extended Mie's scattering theory. An optimized absorption power of these hollow spheres was quantitatively demonstrated with a large enhanced photocatalytic behavior compared to those without structures under the condition with the same amount of weight as solid spheres. Our results demonstrate the possibility of synthesizing interior structure in nano-materials for applications in green energy and dye sensitized solar cell with TiO_2 nano-particles.

Acknowledgment

The authors would like to thank the National Science Council of the Republic of China, Taiwan, for financially supporting this research under Contract No. NSC 101-2113-M-007-012-MY3 and NSC 101-2811-M-032-013.

Appendix A. Supplementary data

Supplementary data associated with this article can be found, in the online version, at http://dx.doi.org/10.1016/j.apcatb.2013.09.033.

References

[1] M.-C. Tsai, J.-C. Chang, H.-S. Sheu, H.-T. Chiu, C.-Y. Lee, Chem. Mater. 21 (2009) 499–505.
[2] P.-C. Chen, M.-C. Tsai, H.-C. Chen, I.-N. Lin, H.-S. Sheu, Y.-S. Lin, J.-G. Duh, H.-T. Chiu, C.-Y. Lee, J. Mater. Chem. 22 (2012) 5349–5355.
[3] A. Ghicov, M. Yamamoto, P. Schmuki, Angew. Chem. Int. Ed. 47 (2008) 7934–7937.
[4] M.-H. Yang, T.-T. Chen, Y.-S. Wang, H.-T. Chiu, C.-Y. Lee, J. Mater. Chem. 21 (2011) 18738–18743.
[5] M.C. Tsai, T.L. Tsai, C.T. Lin, R.J. Chung, H.S. Sheu, H.T. Chiu, C.Y. Lee, Anal. Chem. 81 (2009) 7590–7596.
[6] B. Jones, M. Vergne, D. Bunk, L. Locascio, M. Hayes, Anal. Chem. 79 (2007) 1327–1332.
[7] R. Asahi, T. Morikawa, T. Ohwaki, K. Aoki, Y. Taga, Science 293 (2001) 269–271.
[8] O. Carp, C. Huisman, A. Reller, Prog. Solid State Chem. 32 (2004) 33–177.
[9] M.-H. Yang, P.-C. Chen, M.-C. Tsai, T.-T. Chen, I.-C. Chang, H.-T. Chiu, C.-Y. Lee, CrystEngComm 15 (2013) 2966–2971.
[10] K. Shankar, J.I. Basham, N.K. Allam, O.K. Varghese, G.K. Mor, X.J. Feng, M. Paulose, J.A. Seabold, K.S. Choi, C.A. Grimes, J. Phys. Chem. C 113 (2009) 6327–6359.
[11] G.K. Mor, K. Shankar, M. Paulose, O.K. Varghese, C.A. Grimes, Nano Lett. 5 (2005) 191–195.
[12] T.Y. Ke, C.-Y. Lee, H.-T. Chiu, Appl. Catal. A: Gen. 381 (2010) 109–113.
[13] G.-H. Li, K.A. Gray, Chem. Phys. 339 (2007) 173–187.
[14] M.-H. Yang, M.-C. Tsai, Y.-W. Chang, Y.-C. Chang, H.-T. Chiu, C.-Y. Lee, ChemCatChem 5 (2013) 1871–1876.
[15] A. Sclafani, J.M. Herrmann, J. Photochem. Photobiol. A: Chem. 113 (1998) 181–188.
[16] M.K. Seery, R. George, P. Floris, S.C. Pillai, J. Photochem. Photobiol. A: Chem. 189 (2007) 258–263.
[17] P.D. Cozzoli, R. Comparelli, E. Fanizza, M.L. Curri, A. Agostiano, D. Laub, J. Am. Chem. Soc. 126 (2004) 3868–3879.
[18] J.G. Yu, J.F. Xiong, B. Cheng, S.W. Liu, Appl. Catal. B: Environ. 60 (2005) 211–221.
[19] A. Patsoura, D.I. Kondarides, X.E. Verykios, Appl. Catal. B: Environ. 64 (2006) 171–179.
[20] T.C. Jagadale, S.P. Takale, R.S. Sonawane, H.M. Joshi, S.I. Patil, B.B. Kale, S.B. Ogale, J. Phys. Chem. C 112 (2008) 14595–14602.
[21] D. Dvoranova, V. Brezova, M. Mazur, M.A. Malati, Appl. Catal. B: Environ. 37 (2002) 91–105.
[22] H. Irie, Y. Watanabe, K. Hashimoto, Chem. Lett. 32 (2003) 772–773.
[23] T. Ohno, M. Akiyoshi, T. Umebayashi, K. Asai, T. Mitsui, M. Matsumura, Appl. Catal. A: Gen. 265 (2004) 115–121.
[24] C.F. Bohren, D.R. Huffman, Absorption and Scattering of Light by Small Particles, Wiley, New York, 1983.
[25] H.X. Li, Z.F. Bian, J. Zhu, D.Q. Zhang, G.S. Li, Y.N. Huo, H. Li, Y.F. Lu, J. Am. Chem. Soc. 129 (2007) 8406–8407.
[26] X.Y. Lai, J. Li, B.A. Korgel, Z.H. Dong, Z.M. Li, F.B. Su, J.A. Du, D. Wang, Angew. Chem. Int. Ed. 50 (2011) 2738–2741.
[27] J.F. Chen, H.M. Ding, J.X. Wang, L. Shao, Biomaterials 25 (2004) 723–727.
[28] H. Xu, X. Chen, S.X. Ouyang, T. Kako, J.H. Ye, J. Phys. Chem. C 116 (2012) 3833–3839.
[29] J.G. Yu, X.X. Yu, Environ. Sci. Technol. 42 (2008) 4902–4907.
[30] J.G. Yu, W. Liu, H.G. Yu, Cryst. Growth Des. 8 (2008) 930–934.
[31] J.G. Yu, S.W. Liu, H.G. Yu, J. Catal. 249 (2007) 59–66.
[32] G. Dai, L. Zhao, J. Li, L. Wan, F. Hu, Z. Xu, B. Dong, H. Lu, S. Wang, J. Yu, J. Colloid Interface Sci. 365 (2012) 46–52.
[33] F. Zhu, D. Wu, Q. Li, H. Dong, J. Li, K. Jiang, D. Xu, RSC Adv. 2 (2012) 11629–11637.
[34] X.P. Lin, D.M. Song, X.Q. Gu, Y.L. Zhao, Y.H. Qiang, Appl. Surf. Sci. 263 (2012) 816–820.
[35] M.C. Tsai, T.L. Tsai, C.T. Lin, R.J. Chung, H.S. Sheu, H.T. Chiu, C.Y. Lee, J. Phys. Chem. C 112 (2008) 2697–2702.
[36] R. Jenkins, R.L. Snyder, Introduction to X-ray Powder Diffractometer in Chemical Analysis, Wiley, New York, 1996.
[37] Z.F. Zhu, Z.L. He, J.Q. Li, J.Q. Zhou, N. Wei, D.G. Liu, J. Mater. Sci. 46 (2011) 931–937.
[38] H.G. Yang, H.C. Zeng, J. Phys. Chem. B 108 (2004) 3492–3495.
[39] J.G. Yu, L. Shi, J. Mol. Catal. A: Chem. 326 (2010) 8–14.
[40] G.S. Wu, J.P. Wang, D.F. Thomas, A.C. Chen, Langmuir 24 (2008) 3503–3509.
[41] P.W. Voorhees, J. Stat. Phys. 38 (1985) 231–252.
[42] T. Threlfall, Org. Process Res. Dev. 7 (2003) 1017–1027.
[43] Y.J. Kim, M.H. Lee, H.J. Kim, G. Lim, Y.S. Choi, N.G. Park, K. Kim, W.I. Lee, Adv. Mater. 21 (2009) 3668–3673.
[44] W.G. Yang, F.R. Wan, Q.W. Chen, J.J. Li, D.S. Xu, J. Mater. Chem. 20 (2010) 2870–2876.
[45] Y.W. Jun, M.F. Casula, J.H. Sim, S.Y. Kim, J. Cheon, A.P. Alivisatos, J. Am. Chem. Soc. 125 (2003) 15981–15985.
[46] H.G. Yang, G. Liu, S.Z. Qiao, C.H. Sun, Y.G. Jin, S.C. Smith, J. Zou, H.M. Cheng, G.Q. Lu, J. Am. Chem. Soc. 131 (2009) 4078–4083.
[47] H.-G. Yang, C.-H. Sun, S.-Z. Qiao, J. Zou, G. Liu, S.-C. Smith, H.-M. Cheng, G.-Q. Lu, Nature 453 (2008) 638–641.
[48] H.M. Zhang, Y. Wang, P.R. Liu, Y.H. Han, X.D. Yao, J. Zou, H.M. Cheng, H.J. Zhao, ACS Appl. Mater. Inter. 3 (2011) 2472–2478.
[49] A.L. Aden, M. Kerker, J. Appl. Phys. 22 (1951) 1242–1246.